ADVANCES IN MATERIALS SCIENCE, Vol. 25, No. 4 (86), December 2025

DOI: 10.2478/adms-2025-0023

Michał Landowski [1*], Adrian Wolski [1], Sebastian Stano [2], Grzegorz Chrobak [2]

[1] *Institute of Manufacturing and Materials Technology, Faculty of Mechanical Engineering and Ship Technology, Gdańsk University of Technology, Gdańsk, Poland*
[2] *IPG Photonics Sp. z o.o., Gliwice, Poland*

**michal.landowski@pg.edu.pl Orcid ID: 0000-0002-7926-9410*

INFLUENCE OF LASER BEAM OSCILLATION ON WELD GEOMETRY AND MICROSTRUCTURE OF AISI 304 STAINLESS STEEL

ABSTRACT

Laser welding, thanks to the use of oscillating heads, is finding increasing use in modern industry. Laser oscillating welding heads offer numerous advantages over traditional laser welding heads. Currently, industries where preparing components for laser welding was previously a significant challenge can now adopt this welding technique thanks to the use of oscillation. The ability to improve the properties of welded joints, autogenous welding, and a high level of process automation make laser welding technology a promising industry. Unfortunately, the complexity of multidimensional processes, already difficult to apply, combined with the wide range of possibilities for modifying beam oscillation, requires a deeper understanding of the impact of new laser welding parameters on the quality of welded joints for industrial implementation. This article presents the results of studies on the microstructure of austenitic stainless steel welded with a laser beam at various welding beam oscillation parameters. The welds were obtained using a ytterbium QCW (Quasi Continuous Wave) fiber laser autogenous (without the use of the filler material). The test material was 4 mm thick AISI 304 austenitic stainless steel sheets as delivered. The aim of this study was to investigate the effect of oscillation parameters such as frequency, amplitude, and shape used during laser welding on weld geometry. Statistical relationships between the studied variables were identified. Laser power exhibits strong positive correlations with key weld geometry parameters, particularly penetration depth (H: $r = 0.66$), weld face width (B: $r = 0.79$), and cross-sectional area (S: $r = 0.80$). In contrast, laser beam oscillation parameters show a negative correlation with penetration depth (H: $r = -0.48$) and a moderate correlation with weld face width (B: $r = 0.56$). Other oscillation related effects demonstrate only weak correlations ($r \leq 0.38$) with weld geometry. Mathematical models describing these relationships were developed and their quality verified. The presented models enable the prediction of the transverse shape dimensions of welds based on known welding parameter values.

Keywords: *laser welding; stainless steel; oscillation; weld geometry; statistical analysis*

INTRODUCTION

Laser beam technologies constitute a major development trend in modern manufacturing and have found widespread application in numerous industrial fields. The exceptional combination of properties that characterize lasers as engineering tools has led to their

Received: 13.09.2025; Received in revised form: 19.12.2025; Accepted: 22.12.2025

widespread adoption both as replacements for conventional technologies and for the development of novel applications [1, 2]. Among the many innovative uses of laser beams, the following may be identified: welding, brazing, cladding, cutting, surface heat treatment, drilling, marking, surface structuring, and other advanced material processing technologies[3–6]. Lasers are also used as heat sources for hybrid welding and the currently highly developed additive manufacturing [7].

Laser welding, due to its numerous advantages, is increasingly being selected as an alternative to arc welding processes. Significantly higher welding speeds, the possibility of welding without filler material, a narrow heat affected zone (HAZ), and minimal post-weld distortions resulting from the narrow weld seam are undeniable benefits of this method [8, 9]. However, laser welding is not limited to advantages only. High welding speeds and small weld dimensions result in extremely rapid solidification and cooling of the joint, which can cause problems with some materials [10–12]. Finding the right range of essential process variables is not easy. A number of parameters influence the occurrence of welding defects, such as underfill, undercut, root hump, porosity, and others [13–15].

Laser welding also requires highly precise preparation of the joined components. This is particularly critical in autogenous laser welding processes - welding without the use of filler material [16–18]. The very narrow tolerance results from focusing the laser beam onto an extremely small area. This is especially important during deep penetration laser welding, known as keyhole mode.

Recognizing the potential of laser technologies in many manufacturing sectors, manufacturers are increasingly deciding to switch from arc welding methods to laser beam welding [19, 20]. Unfortunately, the preparation of components for welding often differs significantly from the requirements of laser welding - the tolerances of the joints often result in excessively large gaps, preventing the focused laser beam from properly melting the edges of the joined components [21, 22].

Laser technologies are currently the subject of intensive research aimed at developing new solutions and optimizing existing ones [23]. Solutions are emerging that enable heat treatment or cleaning before or after welding - multi-beam heads [24], scanning heads that allow beam deflection to correct the trajectory, or the latest solutions enabling live measurement of weld penetration depth. Manufacturers of modern laser welding heads, responding to the growing range of laser welding applications, are equipping their process heads with beam oscillation mechanisms [25, 26]. This oscillation mechanism allows for wider welds while maintaining the small heat-affected zone characteristic of laser welding [27, 28].

Currently, methods are being developed to control weld penetration by oscillating the beam to ensure, for example, a sufficiently large weld area in thin materials, which is particularly important in the battery industry [29]. Currently introduced single-mode lasers with highly focused beams enable significantly increased penetration depths. Unfortunately, such a focused beam is highly susceptible to improper surface preparation of the joined components, and creating butt joints without oscillation would be a significant challenge. The effect of beam oscillation on weld formation is also being exploited in manual laser welding systems, enabling the transition from automated, high-precision laser welding to less precise manual processing while maintaining acceptable weld properties [30, 31]. Some studies have found that incorporating oscillations into the process reduces the porosity of welds made using a laser beam. Wang [32], while examining the effect of oscillations during laser welding on the microstructure of an aluminium alloy, achieved a porosity reduction from 40% to 35% using linear oscillation, to 23% using circular oscillation, and even to approximately 2% using infinity oscillation. Zang [33] studies have shown varying effects of frequency and amplitude

on the stabilization of the keyhole cavity filled with metal vapor during deep penetration welding. Results were presented for welding over a wide frequency range and demonstrated that increasing the beam oscillation frequency contributes to reduced weld porosity.

Manufacturers of laser heads and laser sources develop various oscillation patterns and amplitudes which, combined with the capability to operate over a wide range of oscillation frequencies — up to 1 kHz — may generate potential challenges in determining the often non-obvious geometry of the resulting weld [34]. Therefore, it is essential to determine how the oscillation pattern and frequency influence the geometry of the weld and deep of penetration.

Stainless steels are frequently used in the construction of machine parts and devices in many industries, not only because of their corrosion resistance. Thanks to their mechanical properties and resistance to temperatures ranging from high to extremely low, austenitic stainless steels are often chosen as special-purpose construction materials [35]. Austenitic steels are characterized by a stable single-phase austenitic microstructure over a wide temperature range. This structural stability translates into favourable high temperature properties, including good resistance to creep and oxidation. As a result, selected austenitic grades such as AISI 304H and 316Ti, as well as high-alloy cast materials like Manaurite XM [36], are commonly applied in components operating at temperatures exceeding 600 °C [37, 38], for example in petrochemical furnaces, heat-treatment equipment, and power-generation systems [39]. In contrast, conventional low-carbon austenitic grades such as AISI 304L, while offering excellent corrosion resistance at ambient and moderately elevated temperatures, are less suitable for prolonged service above 600 °C due to their limited creep strength. Ferritic and martensitic stainless steels, on the other hand, tend to suffer from microstructural degradation at elevated temperatures. Accelerated diffusion processes in these materials promote carbide coarsening, recovery and recrystallization of the martensitic structure, and rapid loss of mechanical strength, which significantly limits their applicability in long-term high-temperature service compared to austenitic steels [40, 41]. Laser welding of austenitic steels is the subject of numerous scientific studies [42, 43]. Studies have been conducted on similar [44] and dissimilar joints [16, 45], welding with [46] and without filler material, and the influence of shielding gas on the laser welding process [47, 48]. In addition to material variables, the impact of using various types of laser beam sources and processes on the properties and microstructure of austenitic steel joints has been investigated. In their study, Farhadipour [49] investigated the effect of oscillations on the microstructure of austenitic steel and the resulting changes in the mechanical properties of welded joints. They determined that the oscillation amplitude has a significant effect on increasing the strength of the joints.

Despite the growing interest in laser beam oscillation techniques for welding austenitic stainless steels, most published studies focus primarily on qualitative observations of weld morphology and microstructural evolution. In the present work, a systematic and statistically supported analysis of weld penetration geometry is proposed, with particular emphasis on the influence of laser beam oscillation parameters such as frequency, amplitude, and oscillation pattern. The novelty of this study lies in the quantitative correlation between oscillation characteristics and key geometric features of the fusion zone, supported by statistical evaluation of experimental data, providing a more rigorous basis for process optimization than previously reported qualitative approaches. In this study, a statistical analysis was performed to investigate the influence of selected laser welding parameters on the weld penetration characteristics of AISI 304 stainless steel and to establish mathematical relationships between the process parameters and weld properties. To the best of the authors' knowledge, this type of analysis has not yet been reported in the literature.

MATERIALS AND METHODS

Material

The test material was a flat plates with thickness of 4 mm made of austenitic stainless steel grade AISI 304 (X5CrNi18-10 / 1.4301) in delivery condition. The chemical composition (Table 1) was subjected to examination using optical emission spectroscopy Bruker AXS. Comparison with the requirements of the standard EN 10088-3 regarding chemical composition shows that the tested material has a chemical composition in accordance with the standard.

Table 1. *Chemical composition of 304 (1.4301)*

Element	C	Cr	Ni	Mo	Mn	Si	Cu	P	S	Fe
wt.%	0.024	18.71	8.64	0.41	1.52	0.62	0.38	0.034	0.005	bal.

Laser welding setup and beam oscillation strategy

A diode-pumped ytterbium fiber laser IPG Photonics YLR – 450/4500 QCW with a maximum power of 450 W in continuous mode and 4.5 kW in pulse mode and a wavelength of 1070 nm was used. Two main modes of laser emission were possible: continuous (called Continuous Wave, CW) and pulsed mode. In this study, CW emission was chosen to determine the effect of beam oscillations. The bead on plate welds were made at laser output power of 450 W and in 80%, 60% 40% power for some experiments. The laser beam was delivered through the optical feeding fiber (transmitting fiber) of 50 μm core diameter. The D30 wobbler with air cooled controller welding head (Fig. 1a) was used with a focal length of the collimator lens and the focusing lens of 100 and 200 μm, respectively. This optical system provides a spot diameter of approximately 100 μm. The IPG D30 head is equipped with a system of mirrors that can oscillate the beam on the surface of the workpiece. The basic wobbling modes available in the head's software include circular (clockwise and counterclockwise), linear, figure-eight, and infinity patterns. The maximum oscillation amplitude of the patterns is directly proportional to the focal length of the focusing lens, while the maximum oscillation frequency (1 kHz) decreases to about 260 Hz as the amplitude increases. For the applied focusing lens with a 200 mm focal length, the maximum amplitude reaches 6 mm. In these studies, it was decided to use a circular figure-eight and an infinity sign - an example of the appearance of the trajectory and the melted surface is visible in Figure 1b.

During welding high-purity argon shielding gas (I1) was supplied through a coaxial nozzle integrated with the welding head along the laser beam axis. This nozzle has a telescopic option that allows for length changes, ensuring the appropriate shielding gas flow regardless of the adjustable distance between the head and the workpiece, which is used to change the beam focus position. The nozzle diameter was 9 mm and the shielding gas flow was set to 12 l/min. Motion was achieved by an automated cartesian table on which the sample was mounted relative to a stationary head. All tests were performed at a constant travel speed (1 m/min) to minimize the influence of factors other than beam oscillation.

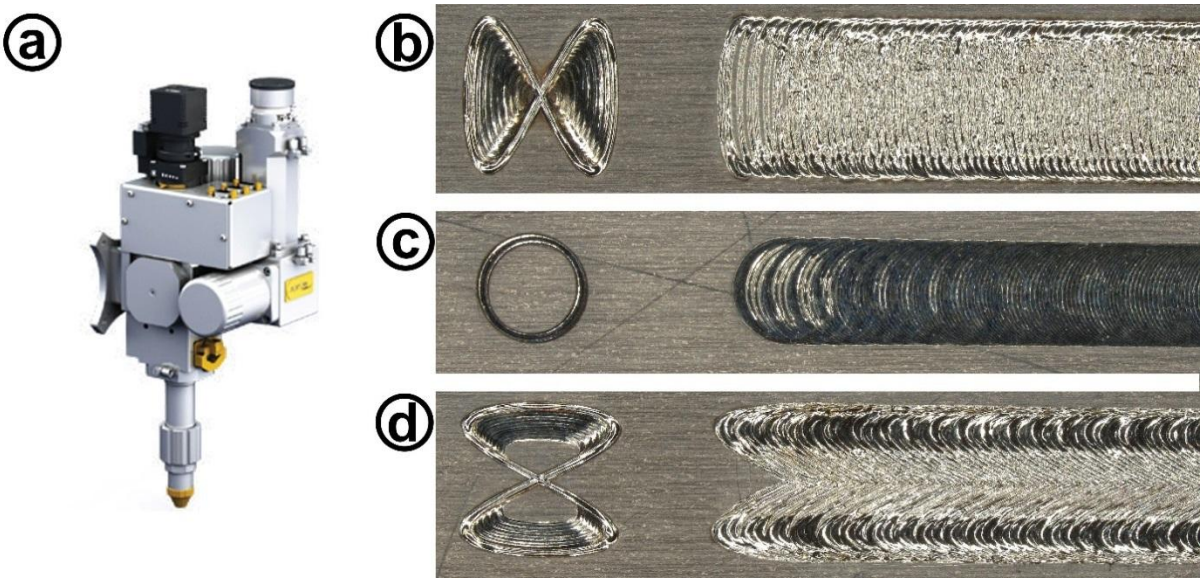

Fig. 1. IPG D30 wobble welding head (a), oscillation modes "∞" (b), "o" (c), "8" (d)

Metallographic examination

The samples for metallographic examination were cut at the cutting machine with intensive cooling to prevent changes in the structure of the material under the influence of temperature during cutting. Samples were mounted in epoxy resin and ground on aqueous abrasive papers with increasing granularity from 600 to 2400 for microscopic examinations. Samples for microscopic observation were polished on a polishing cloth successively using an aqueous suspension of 6 and 3 μm Al_2O_3. The metallographic samples thus prepared were subjected to hot etching solution (3 ml HNO_3, 1 ml HF and 50 ml H_2O in 70 °C) to reveal the microstructure of the joints in macroscopic and microscopic studies. Structural and macroscopic observations were carried out using light microscopy (Olympus BX51) and digital microscope (Keyence VHX-7000).

Experimental design and process parameter grouping

The values of the independent variables were determined based on preliminary investigations and the authors' prior experimental work, with the objective of encompassing the broadest feasible range of their variability. The welded path length was 70 mm, which, according to previous studies, was sufficient to stabilize the process, ensuring a long, stable measurement section. Groups of samples were tested according to the appropriate schemes. The first group was a control group – without oscillations and with circular oscillations at various power levels (100%, 80%, 60%, and 40% - see Table 2). Due to the very small penetration at 40% power, further testing at this power level was discontinued.

An example macroscopic image showing the appearance of the fusion line shape using 100% laser power without oscillations and with circular oscillation at a frequency of 300 Hz for different oscillation amplitudes is shown in Figure 2. The typical "chalice" or "wine glass" shaped shape of a laser weld performed with deep penetration, i.e., keyhole welding, can be observed [50, 51]. This shape widens for welding with low amplitude oscillation compared to welding without oscillation. At higher amplitudes, the characteristic fusion line shape disappears, and uneven penetration depth is visible, resulting from the vector summation of the welding speed and oscillation speed.

Table 2. *First control group – circular oscillation, amplitude and laser power*

Number	Wobbling type	Amplitude	Power	Number	Wobbling type	Amplitude	Power
1_1	None	None	450 W	3_1	circular	0.8 mm	450 W
1_2	None	None	360 W	3_2	circular	0.8 mm	360 W
1_3	None	None	270 W	3_3	circular	0.8 mm	270 W
1_4	None	None	180 W	3_4	circular	0.8 mm	180 W
2_1	circular	0.5 mm	450 W	4_1	circular	1.1 mm	450 W
2_2	circular	0.5 mm	360 W	4_2	circular	1.1 mm	360 W
2_3	circular	0.5 mm	270 W	4_3	circular	1.1 mm	270 W
2_4	circular	0.5 mm	180 W	4_4	circular	1.1 mm	180 W

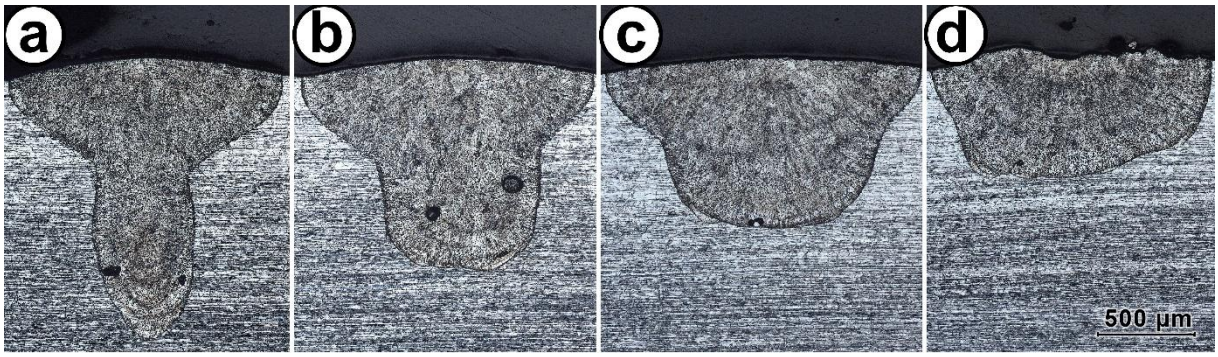

Fig. 2. Weld shape power level 100% without oscillation (a), with circle oscillation amplitude 0.5 (b), 0.8 (c) and 1.1 mm (d), magn. x100

Further experiments were conducted using various types of oscillations eight and the infinity symbol, as well as various variations of oscillation amplitude (Table 4) and frequency (Table 5), but only at the 100% power level. In order to obtain a comprehensive assessment of the influence of oscillation parameters on the dimensions and shape of the weld, a statistical analysis of the obtained results was performed.

The oscillation trajectory of the laser beam was treated as a qualitative variable (variable "M"), with categories assigned to specific shapes: none (no oscillation), eight (trajectory in the shape of a eight number, 8), circle (circular trajectory, O), and infinity (trajectory in the shape of the infinity symbol, ∞).

Statistical analyses were performed using the Statistica software package, assuming a significance level of 0.05, through the development and evaluation of various mathematical models obtained via regression methods. The agreement of the raw residuals with the normal distribution was assessed both statistically, using the Shapiro–Wilk test, and graphically, by examining the normal probability plot. Furthermore, heteroscedasticity was examined visually by inspecting plots of observed variables against raw residuals [52].

The qualitative variable M (oscillation type: none, eight, circle, infinity) was converted into dummy variables. The category "none" was selected as the reference category, while three dummy variables (M_eight, M_circle, and M_infinity) were created for the remaining categories, taking variables of 0 or 1 depending on the sample's membership in the respective category. These dummy variables were included in the regression analysis to account for the effect of oscillation type on the dependent variable.

Due to the multivariate nature of welding processes, several methodological approaches to regression analyses were performed, including multiple regression, polynomial regression, Response Surface Methodology (RSM) and the best subset model selection approach. In this case, the adjusted coefficient of determination was used as the selection criterion.

Table 3 presents the nomenclature used for the weld geometry and laser welding parameters in this study.

Table 3. *Nomenclature of weld geometry and laser welding parameters*

Symbol	Parameter	Unit
H	penetration depth	µm
R	weld reinforcement height	µm
B	weld face width	µm
S	weld cross-sectional area	µm²
P	laser power	W
A	laser beam oscillation amplitude	mm
f	oscillation frequency	Hz
M	oscillation mode	0 / 1 / 2 / 3

Table 4. *Second group "amplitude"– eight and infinity oscillation and 450 W laser power*

Number	Wobbling type	Amplitude	Frequency	Number	Wobbling type	Amplitude	Frequency
5_1	Infinity	0.5 mm	300 Hz	6_1	Eight	0.5 mm	300 Hz
5_2	Infinity	1.0 mm	300 Hz	6_2	Eight	1.0 mm	300 Hz
5_3	Infinity	0.8 mm	300 Hz	6_3	Eight	0.8 mm	300 Hz
5_4	Infinity	1.1 mm	300 Hz	6_4	Eight	1.1 mm	300 Hz
5_5	Infinity	1.4 mm	300 Hz	6_5	Eight	1.4 mm	300 Hz
5_6	Infinity	1.7 mm	300 Hz	6_6	Eight	1.7 mm	300 Hz

Table 5. *Third group "frequency" – eight, infinity and circular oscillation and 450 W laser power*

Number	Wobbling type	Amplitude	Frequency	Number	Wobbling type	Amplitude	Frequency
7_1	Eight	0.5 mm	50 Hz	8_1	Infinity	0.5 mm	50 Hz
7_2	Eight	0.5 mm	100 Hz	8_2	Infinity	0.5 mm	100 Hz
7_3	Eight	0.5 mm	200 Hz	8_3	Infinity	0.5 mm	200 Hz
7_4	Eight	1.1 mm	50 Hz	8_4	Infinity	1.1 mm	50 Hz
7_5	Eight	1.1 mm	100 Hz	8_5	Infinity	1.1 mm	100 Hz
7_6	Eight	1.1 mm	200 Hz	8_6	Infinity	1.1 mm	200 Hz
9_1	Circular	0.5 mm	50 Hz	9_4	Circular	1.1 mm	50 Hz
9_2	Circular	0.5 mm	100 Hz	9_5	Circular	1.1 mm	100 Hz
9_3	Circular	0.5 mm	200 Hz	9_6	Circular	1.1 mm	200 Hz

RESULTS AND DISCUSSION

Macroscopic examination

Due to the large number of welds performed, representative images of only selected parameters were presented in the following study. Only the appearance of the weld bead due to incomplete penetration was analysed as one of the geometric parameters. Figure 3 shows a sample set of images for selected parameters of different welding oscillation amplitudes compared to welding without oscillation. It was observed that amplitude affects the stabilization of the weld bead width. Using a higher amplitude of 1.1 mm compared to no oscillation or circular oscillation with an amplitude of 0.5 mm allowed for comparable weld bead quality for all oscillation types. It is also possible to observe that even at lower amplitudes, such as 0.5 mm, the figure of eight oscillation allows stabilization of the weld bead geometry at a level only achievable at higher amplitudes for other oscillation shapes, such as circular or infinity.

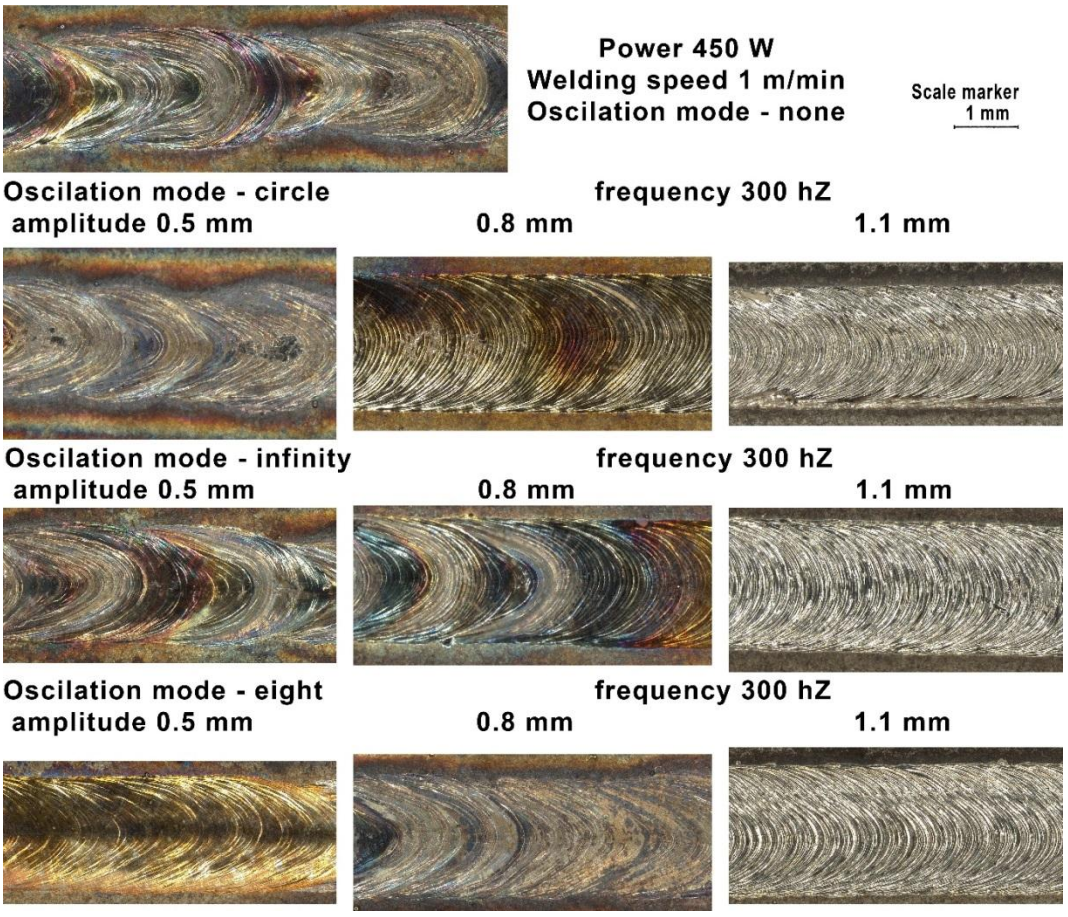

Fig. 3. Appearance of the weld face for different amplitudes and oscillation patterns, magn. x50

Three types of oscillations were used during the tests, with both the amplitude and frequency of the oscillation varied. Figure 4 shows the effect of oscillation frequency on the appearance of the weld bead for the three types of oscillations at an amplitude of 0.5 mm. It can be observed that low frequencies of around 50 Hz do not ensure stable weld bead formation. As with different amplitudes, the best behaviour of the melted metal is observed for eight shape oscillations. Increasing the amplitude to 200 or 300 Hz allows for a more stable appearance of the weld bead, not only due to its width.

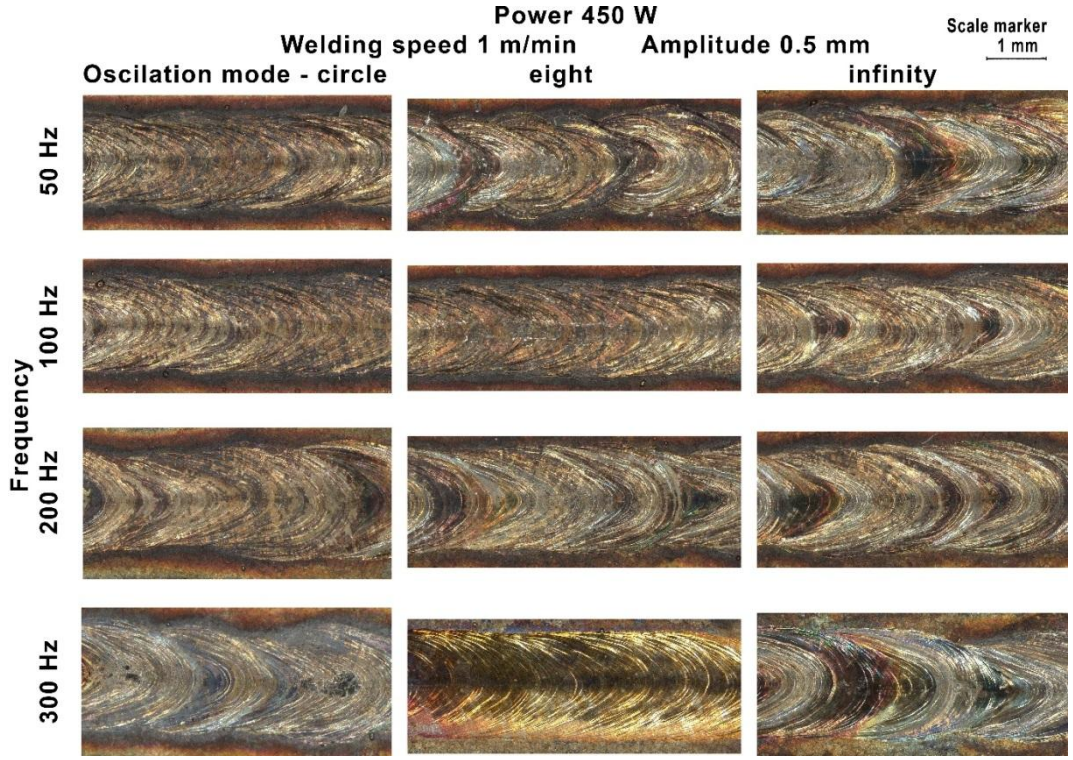

Fig. 4. Appearance of the weld face for different frequency and oscillation patterns, magn. x50

The tests carried out also showed non-obvious differences in the appearance of the weld face and also in the cross sections. To demonstrate the difference, the same amplitude and oscillation frequency were selected at 1.7 mm and 300 Hz, respectively. Although the oscillation shape is identical, with only a 90° rotation of the shape, the results are different. This was already visible in the appearance of the weld bead at lower amplitude parameters and the stabilization of the weld bead width. The appearance of the weld bead, as well as the cross section, show differences in the formation of penetration, as shown in Figure 5. The differences result from the direction of beam movement and the addition or subtraction of the resultant velocity associated with the oscillation from the welding speed (main motion).

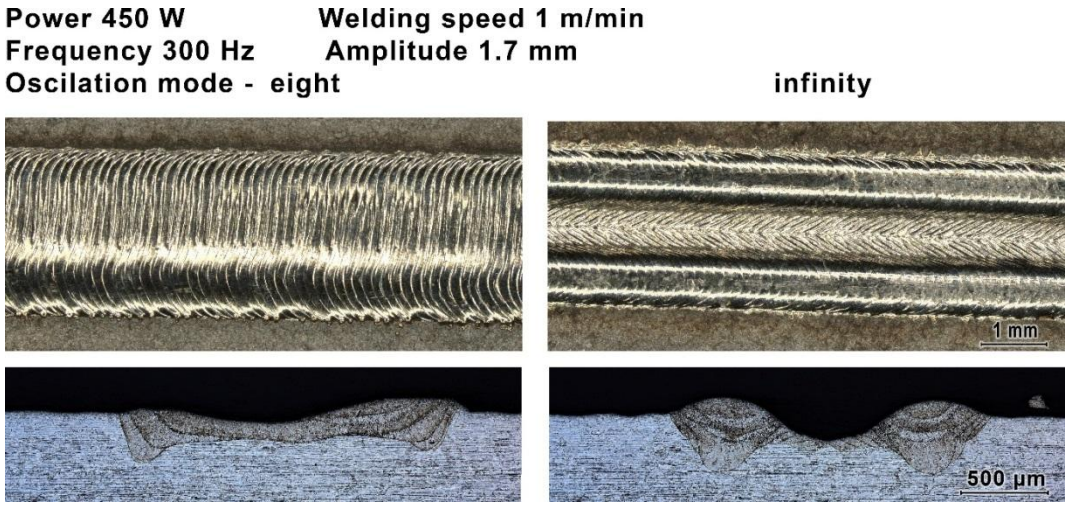

Fig. 5. Appearance of the weld face for different frequency and oscillation patterns, magn. x100

Microscopic examination

The effect of oscillations on the appearance of the face, as well as its repeated crystallization and remelting, can also cause microstructural changes. The material considered in these studies, austenitic steel, exhibits a very narrow heat affected zone, which means that changes in the microstructure of the melted material can be more easily observed. The phase solidification characteristics could occur in the ratio of Cr:Ni of the 304 were approximately 18.71 wt% Cr, 8.64 wt% Ni, and 69 wt% Fe corresponding in Table 1. The chemical compositions were marked as red line showing the solidification path according to the Fe-Cr-Ni pseudo-binary phase diagram which represents the solidification path position in Figure 6(a).

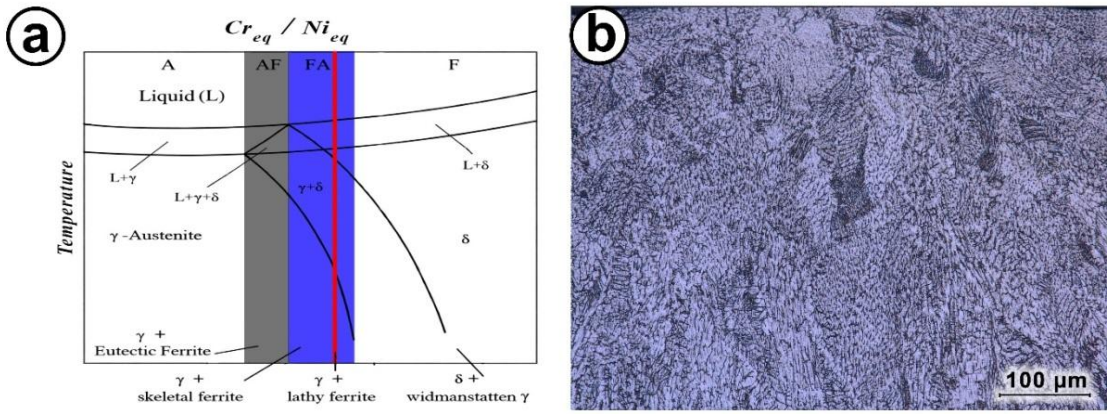

Fig. 6. Fe-Cr-Ni pseudo-binary phase diagram for the microstructure prediction of (Fe 70%) 304 stainless steel (a), microstructure of weld (middle zone) 100% power without oscillation (b), magn. x500

Therefore, the behaviour of the melted material during solidification is presented according to the FA scheme – first, crystallization begins with the formation of primary ferrite, followed by the formation of austenite in a peritectic reaction. Subsequently, due to the reduced stability of the ferrite phase during cooling, the ferrite phase transforms into the austenite phase through diffusion transformation [53]. Diffusion also causes an increased content of ferrite forming elements in certain areas of the ferrite, causing its stabilization and, consequently, its retention in the structure after the joint has cooled completely [54]. The forming austenite is distributed at the boundaries of dendrites and ferrite grains. The amount of austenite depends on the crystallization conditions and the Cr_{eq} to Ni_{eq} ratio. High cooling rates reduce diffusion to small distances, resulting in the formation of a lath-like ferrite (finer and more tightly packed) [55]. Slower heat dissipation allows for diffusion over longer distances, resulting in the formation of skeletal ferrite. Figure 6b shows the microstructure of the central part of the weld made without oscillation at 100% laser power (450 W). A mixed pattern of ferrite formation is visible, with skeletal and lathy ferrite formation.
When characterizing the weld microstructure produced using different circular oscillation frequencies and an amplitude of 0.5 mm, changes in the proportions of ferrite remaining in the structure can be observed in Figure 7. At higher oscillation frequencies, a larger austenite grain size can be observed in the weld, as well as a reduction in the presence of skeletal ferrite and a greater proportion of lath ferrite. The structure of the heat affected zone depends on the initial structure and chemical composition base material. Rapid heating to a temperature close to the solidus and subsequent cooling at various rates can cause various microstructural changes, such as ferrite formation, austenite grain growth, or the initiation of precipitation processes [56].

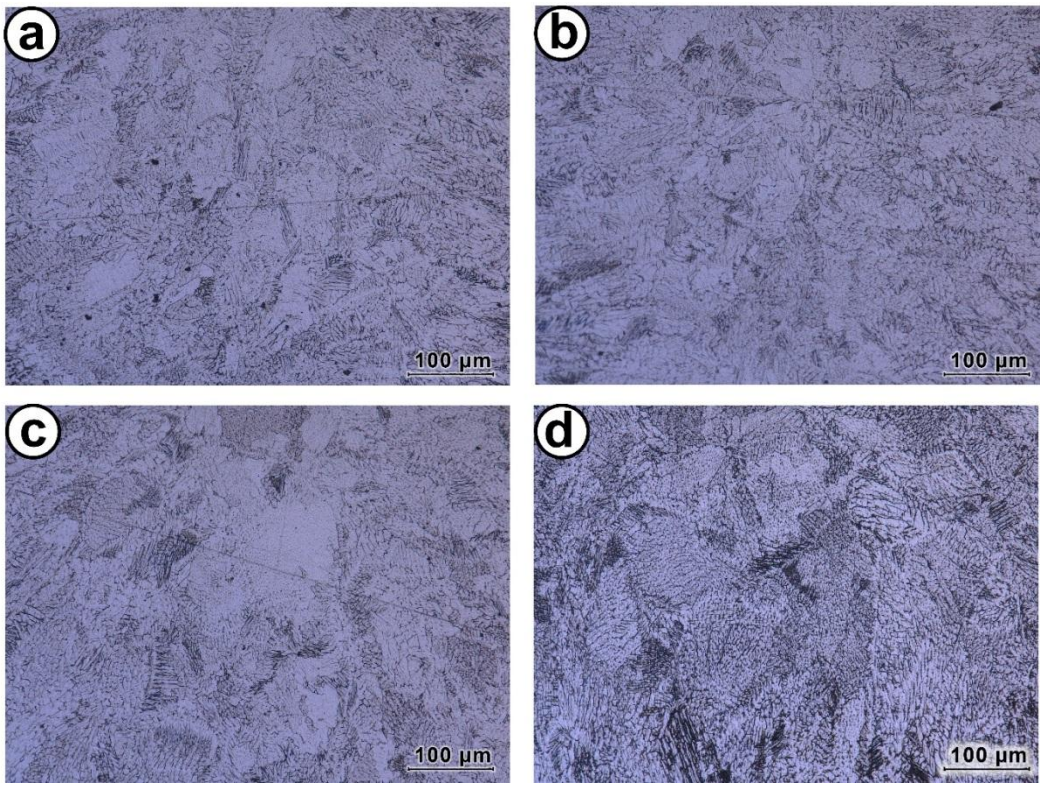

Fig. 7. Near face of weld middle area with circle oscillation amplitude 0.5 mm: 50 Hz (a), 100 Hz (b), 200 Hz (c), 300 Hz (d), magn. x500

When small amounts of heat are introduced into the joint, grain growth in the HAZ structure is usually negligible. High amounts of heat introduced into the joint can cause grain size growth and, consequently, a slight decrease in hardness within the HAZ. When the material is heated to a temperature close to the solidus, which occurs along the fusion line, ferrite precipitates along the austenite grain boundaries. This phenomenon inhibits austenite grain growth [57]. During cooling, the precipitated ferrite can transform into austenite, but it usually remains. The areas shown in Figure 8 were recorded close to the weld face surface, including the fusion line and the HAZ area. Studies on the effect of oscillation showed that increasing the oscillation amplitude in the case of circular oscillation resulted in a decrease in the amount of ferrite precipitated along the fusion line, as seen in Figure 8d, compared to lower amplitude values for Figures 8b and 8c, as well as for the absence of oscillation, as seen in Figure 8a.

Microstructural observations of the heat effect on the area immediately adjacent to the fusion line revealed a reduction in ferrite precipitation in the HAZ. No significant grain growth was observed either. Although the analysis in the present study was based on microstructural observations rather than direct mechanical property measurements, the results allow for a reasoned assessment of the expected mechanical performance of the welded joints. Microstructural examination showed no evidence of excessive grain growth or phase instability in either the heat affected zone or the weld metal, features that are typically associated with the degradation of mechanical properties in welded austenitic stainless steels. Previous studies have demonstrated that specific microstructural characteristics, such as a homogeneous austenitic grain distribution and a controlled ferrite content, correlate well with satisfactory mechanical behaviour of welded joints, even in the absence of extensive mechanical testing [57].

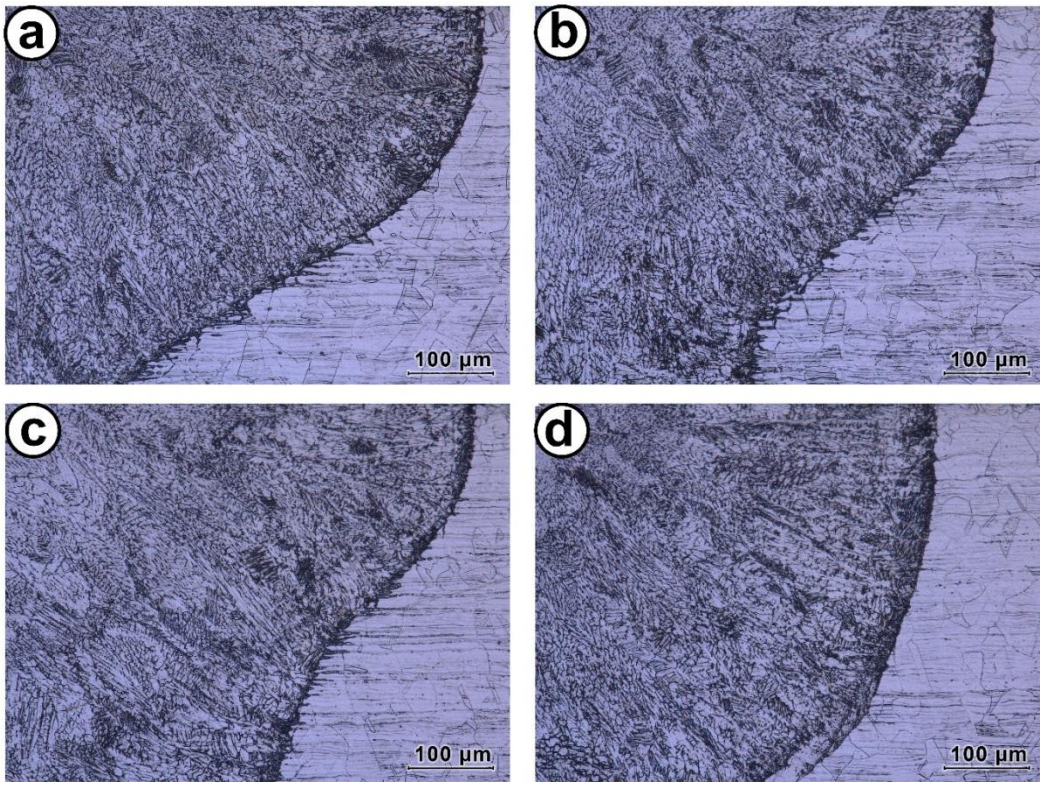

Fig. 8. Near face of weld fusion zone area without oscillation (a), with circle oscillation amplitude 0.5 (b), 0.8 (c) and 1.1 mm (d), magn. x500

For example, investigations on austenitic 304L welds have revealed clear relationships between microstructural heterogeneity and mechanical response across different weld zones [58], while similar studies on hybrid laser/MIG welded 316LN joints confirm that microstructural features significantly influence tensile strength and toughness [59]. Moreover, analyses of laser welded 316L stainless steel indicate that optimized microstructural evolution resulting from appropriate process parameters can maintain mechanical strength at a level comparable to that of the base material [60]. The lack of changes, particularly an increase in HAZ size or grain size in the HAZ, allows for beam oscillation welding to be identified as a more optimal laser welding technique due to the increased weld size – particularly on the root side, which is usually a problem. During observation of metallographic specimens, individual bubbles were observed. In most cases, this confirms literature reports that the number of pores trapped in the weld decreases with increasing oscillation frequency. However, a quantitative assessment was not undertaken because it would require a larger number of metallographic specimens to clearly determine the effect of oscillations. This may also be related to the method of shielding gas delivery – axially into the keyhole. The appearance of varying degrees of oxidation on the sample surfaces may suggest problems with shielding gas delivery to the weld site. Additional studies involving lateral shielding gas delivery could allow for clear conclusions regarding the formation of pores in the weld.

Statistical analyses

Measurements of weld dimensions are presented in Tables 6-8. Keyhole laser welding forms a 'chalice' shaped weld bead profile, which was only observable when welding without oscillation. In the case of welding with oscillation, the geometry was much more complex, and the welding process did not always follow the expected pattern, due to changes in the net velocity of the laser source. For this reason, measurements of some characteristic dimensions

for keyhole welding were omitted and limited to the weld bead width, penetration depth, bead height, and weld cross-sectional area. The weld cross sectional area is defined as the area of the weld metal bounded by the fusion line, excluding the heat affected zone (HAZ).

Table 6. *First group "control" – measurements*

Number	Depth of penetration [μm]	Weld bead heigh [μm]	Weld bead width [μm]	Area of coss-section [μm^2]
1_1	1330	100	1400	965233
1_2	938	77	1088	610555
1_3	570	28	776	260857
2_1	994	87	1495	1032074
2_2	708	47	1253	631269
2_3	402	26	780	252515
3_1	807	70	1607	995071
3_2	540	43	122	537889
3_3	63	21	935	55856
4_1	569	109	1435	744929
4_2	303	51	1274	318631
4_3	30	17	1189	45971

Table 7. *Second group "amplitude"– measurements*

Number	Depth of penetration [μm]	Weld bead heigh [μm]	Weld bead width [μm]	Area of coss-section [μm^2]
5_1	1126	123	1417	1059382
5_2	810	84	1581	939590
5_3	882	81	1552	976260
5_4	736	63	1563	852173
5_5	534	63	1587	598596
5_6	357	92	1804	416790
6_1	1021	103	1462	1049587
6_2	740	67	1579	916198
6_3	908	85	1423	1098494
6_4	638	59	1500	815780
6_5	458	69	1669	581846
6_6	277	47	1927	350892

Table 8. *Third group "frequency"– measurements*

Number	Depth of penetration [μm]	Weld bead heigh [μm]	Weld bead width [μm]	Area of coss-section [μm^2]
7_1	1299	124	1348	1312349
7_2	1196	147	1402	1224797
7_3	1078	112	1419	1074673
7_4	1096	115	1575	1425242
7_5	984	109	1455	1220484
7_6	811	80	1494	1066399
8_1	1344	153	1229	1302517
8_2	1277	195	1191	1266235
8_3	1097	109	1401	1067959
8_4	1085	128	1478	1315031
8_5	961	104	1603	1153904
8_6	873	90	1488	1112600
9_1	1183	160	1488	1190713
9_2	1244	123	1200	1088220
9_3	991	83	1515	994500
9_4	1017	131	1468	1233792
9_5	828	94	1581	1094823
9_6	683	58	1600	904957

Table 9 presents the descriptive statistics and pairwise correlation coefficients for the studied weld geometry and laser welding parameters. Mean values and standard deviations are reported for each variable, reflecting the central tendency and variability of the data. Correlation coefficients indicate the strength and direction of linear relationships between variables, with values close to ±1 representing strong associations and values near 0 representing weak or negligible relationships.

Table 9. *Descriptive statistics and correlation matrix of the variables*

Variable	Mean	Standard deviation	H	R	B	S	P	A	f	M
H	810.2	353.7	1.00	0.85	0.28	0.91	0.66	-0.37	-0.48	0.09
R	86.7	41	0.85	1.00	0.38	0.84	0.69	-0.09	-0.41	0.27
B	1361	354.9	0.28	0.38	1.00	0.46	0.79	0.56	0.21	0.26
S	864240	381748.5	0.91	0.84	0.46	1.00	0.80	-0.04	-0.34	0.21
P	418.6	67.7	0.66	0.69	0.79	0.80	1.00	0.36	0.06	0.30
A	0.8	0.4	-0.37	-0.09	0.56	-0.04	0.36	1.00	0.48	0.38
f	195.3	115.9	-0.48	-0.41	0.21	-0.34	0.06	0.48	1.00	0.34
M	1.8	1	0.09	0.27	0.26	0.21	0.30	0.38	0.34	1.00

Values shown in red font indicate correlations that are statistically significant at the 0.05 significance level, according to the default settings in Statistica. Laser power (P) shows the strongest positive correlations with weld geometry parameters: penetration depth H (r = 0.66), reinforcement height R (r = 0.69), weld face width B (r = 0.79), and cross-sectional area S (r = 0.80), showing larger values of these geometric characteristics at higher power levels. Laser oscillation parameters, amplitude A and frequency f, are negatively correlated with penetration depth H (r = -0.37, -0.48) and moderately correlated with weld face width B (r = 0.56, 0.21). The oscillation pattern M exhibits minimal correlations with most geometric parameters (r ranging from 0.09 to 0.38), but shows some association with amplitude and frequency.

Statistical analyses and a substantive evaluation of their results enabled the development of seven prospective models describing the relationships between laser welding parameters and variables characterizing the weld cross-sectional geometry:

Model I: $H=-1276.83+8.64\cdot P-0.01\cdot P^2+78.99\cdot M_8+126.99\cdot M_\infty-0.53\cdot P\cdot A-1.40\cdot A\cdot f$
Model II: $H=-474.92+3.80\cdot P-564.27\cdot A-1.18\cdot f+419.25\cdot M_8+381.64\cdot M_\circ+467.25\cdot M_\infty$
Model III: $R=-69.60+0.38\cdot P-0.20\cdot f+66.17\cdot M_8+63.27\cdot M_\circ+80.17\cdot M_\infty-0.08\cdot P\cdot A$
Model IV: $B=1004.12+5.87\cdot f-0.02\cdot f^2$
Model V: $B=-322.21+3.50\cdot P+269.18\cdot A$
Model VI: $S=481822.97+982077.55\cdot A-746725.29\cdot A^2+372042.65\cdot M_8+0\cdot M_8^2+$
$+365733.99\cdot M_\infty+0\cdot M_\infty^2$
Model VII: $S=-754887.80+3859.43\cdot P-347608.85\cdot A-1541.87\cdot f+678092.84\cdot M_8+$
$+595543.94\cdot M_\circ+671784.18\cdot M_\infty$

Although the coefficients of M_8^2 and M_∞^2 (model VI) were zero in the selected model, the Pareto chart indicates they have a notable effect, so they were retained for interpretation. This is because the coefficients were set to zero due to the model selection criteria and tolerance limits, rather than a lack of influence on the response variable.

Table 10 presents the types of regression used along with their fit to the experimental results and an assessment of their statistical quality.

Table 10. *Developed regression models and model quality metrics*

Model	Regression type	R	R^2	R^2adj	Normality	Heteroscedasticity
I	RSM with best subset	0.99	0.98	0.98	Met	Met
II	Multiple regression	0.98	0.97	0.96	Met	Met
III	Multiple regression	0.92	0.84	0.81	Violated	Met
IV	Polynomial regression	0.40	0.16	0.12	Violated	Violated
V	Multiple regression	0.84	0.71	0.69	Violated	Violated
VI	Polynomial regression	0.65	0.42	0.36	Met	Met
VII	Multiple regression	0.96	0.92	0.91	Met	Met

The predicted value in a regression model with dummy variables equals the intercept plus the contributions of the continuous predictors and the coefficients of the dummy variables that are equal to 1 for the observation. If not all dummy variables representing a categorical factor are included in the model, the omitted categories jointly form the reference group, and for observations belonging to these categories all corresponding dummy variables take the value 0, while the intercept represents their expected response.

The developed models exhibit different forms and varying quality of fit. The analysis revealed that laser power (P) and oscillation amplitude (A) are the most influential factors affecting the weld geometry. Oscillation patterns (M_8, $M_\circ$, M_∞) also significantly affect the weld parameters, with differences in H, R, and S values depending on the type of oscillation particularly evident in Models I, II, and VII [26]. Interactions between parameters, such as PA and Af (present in Model I), indicate that the effect of one variable depends on the level of another, reflecting the complex mechanisms occurring during welding processes [61]. The highest predictive accuracy was observed for Models I, II, and VII ($R^2 > 0.9$), which can be considered reliable and recommended for predictive purposes. Models III, V, and VI exhibit moderate accuracy and should be interpreted with caution, whereas Model IV, with a very low R^2 (< 0.2), is practically unsuitable for prediction.

CONCLUSIONS

Based on the experimental results and the statistical analysis performed, the following conclusions can be drawn regarding the influence of laser beam oscillation parameters on weld geometry during fiber laser welding of AISI 304 stainless steel:

- The application of regression analysis enabled a quantitative assessment of the influence of laser beam oscillation parameters on weld penetration geometry in AISI 304 stainless steel, allowing general trends to be identified despite variations in oscillation pattern and penetration location.
- An increase in oscillation amplitude led to a nearly linear reduction in penetration depth under the investigated conditions, with the maximum penetration obtained for welding without beam oscillation. At the same time, beam oscillation promoted an increase in weld cross sectional area while limiting excessive widening of the heat affected zone due to repeated remelting and redistribution of heat.
- Beam oscillation significantly modifies the effective melting conditions by altering both the magnitude and direction of the instantaneous beam velocity. This results in locally varying heat input and cooling rates along the weld path, which directly affects weld geometry and solidification behaviour.
- More complex oscillation trajectories, such as figure-eight (infinity) patterns, produced greater penetration depths than circular oscillation despite longer beam paths and higher instantaneous velocities. This effect is attributed to heat accumulation caused by overlapping oscillation trajectories, which compensates for the theoretically lower local heat input.
- The developed regression models and associated equations constitute a novel outcome of this study, providing a statistically supported tool for predicting weld penetration geometry as a function of oscillation frequency, amplitude, and pattern, and offering practical guidance for process optimization in oscillation assisted laser welding.

ACKNOWLEDGMENTS

The authors would like to acknowledge IPG Photonics sp. z o.o. for providing the scientific internship that enabled this study. The authors would like to thank Dariusz Karubin employed at Gdańsk University of Technology for his invaluable technical assistance during the preparation of samples for research.

Ethical Standards
This research was conducted in full compliance with ethical standards. The authors declare that they have no known competing financial interests or personal relationships that could have appeared to influence the work reported in this paper. Michał Landowski serves as an Associate Editor of Advances in Materials Science. He has been excluded from the publication process.

Statement of Research and Publication Ethics
The authors declare that all procedures followed the principles of research integrity and publication ethics.

Conflicts of Interest
The authors declare no conflict of interest regarding the research, authorship, and/or publication of this article.

Funding
This research received no external funding.

REFERENCES

1. Górka J, Suder W, Kciuk M, et al (2023) Assessment of the Laser Beam Welding of Galvanized Car Body Steel with an Additional Organic Protective Layer. Materials 16:. https://doi.org/10.3390/ma16020670
2. Krawczyk J, Pańcikiewicz K, Frocisz Ł, et al (2025) Laser Welding and Remelting of DC05 Low Carbon Steel. Arch Metall Mater 691–699. https://doi.org/10.24425/amm.2025.153470
3. Majkowska-Marzec B, Tęczar P, Bartmański M, et al (2020) Mechanical and Corrosion Properties of Laser Surface-Treated Ti13Nb13Zr Alloy with MWCNTs Coatings. Materials 13:. https://doi.org/10.3390/ma13183991
4. Kwidzińska DB, Jażdżewska M, Fydrych D (2025) The influence of selected metal oxides and laser modification on the surfaces of titanium alloys – Bibliometric and systematic review. Opt Laser Technol 184:112592. https://doi.org/10.1016/j.optlastec.2025.112592
5. Wojdat TK, Piwowarczyk T (2024) Influence of Laser Micro-Texturing and Plasma Treatment on Adhesive Bonding Properties of WC-Co Carbides with Steel. Materials 17:. https://doi.org/10.3390/ma17235999
6. Adamiak M, Czupryński A, Janicki D, Górka J (2016) The causes of high power diode laser brazed seams fractures of dissimilar materials. In: Laser Technology 2016: Progress and Applications of Lasers. SPIE, pp 182–190
7. Adamiec J, Wyciślik-Sośnierz J, Matusiak J, et al (2025) Morphology of Fumes from Hybrid Laser–Arc Welding of X5CrNi18-10 Stainless Steel. Materials 18:5534. https://doi.org/10.3390/ma18245534
8. Janiczak R, Pańcikiewicz K (2021) Laser welding of austenitic ferrofluid container for the KRAKsat satellite. Weld World 65:1347–1357. https://doi.org/10.1007/s40194-021-01103-5
9. Landowski M, Simon SC, Breznay C, et al (2024) Effects of preheating on laser beam–welded NSSC 2120 lean duplex steel. Int J Adv Manuf Technol 130:2009–2021. https://doi.org/10.1007/s00170-023-12840-w
10. Landowski M (2019) Influence of Parameters of Laser Beam Welding on Structure of 2205 Duplex Stainless Steel. Adv Mater Sci 19:21–31. https://doi.org/10.2478/adms-2019-0002

11. Gennari C, Miranda-Pérez AF, Pezzato L, et al (2024) Lean duplex stainless steels welded by LBW subjected to corrosion testing. MRS Adv 9:1887–1890. https://doi.org/10.1557/s43580-024-00981-3
12. Gao W, Wang J, Zhao H, et al (2025) Impact of Welding Heat Input on the Mechanical and Corrosion Properties of Lean Duplex Stainless Steel UNS S32001 Laser-Welded Joints. J Mater Eng Perform 34:13861–13871. https://doi.org/10.1007/s11665-024-10140-2
13. Zhang M, Tang K, Zhang J, et al (2018) Effects of processing parameters on underfill defects in deep penetration laser welding of thick plates. Int J Adv Manuf Technol 96:491–501. https://doi.org/10.1007/s00170-018-1613-x
14. Xu J, Rong Y, Huang Y, et al (2018) Keyhole-induced porosity formation during laser welding. J Mater Process Technol 252:720–727. https://doi.org/10.1016/j.jmatprotec.2017.10.038
15. Kosturek R, Grzelak K, Torzewski J, et al (2022) Microstructure and Mechanical Properties of Sc-Modified AA2519-T62 Laser Beam Welded Butt Joints. Adv Mater Sci 22:57–69. https://doi.org/10.2478/adms-2022-0019
16. Landowski M, Świerczyńska A, Rogalski G, et al (2020) Autogenous Fiber Laser Welding of 316L Austenitic and 2304 Lean Duplex Stainless Steels. Materials 13:. https://doi.org/10.3390/ma13132930
17. Sirohi S, Pandey SM, Tiwari V, et al (2023) Impact of laser beam welding on mechanical behaviour of 2.25Cr–1Mo (P22) steel. Int J Press Vessels Pip 201:104867. https://doi.org/10.1016/j.ijpvp.2022.104867
18. Kurc-Lisiecka A, Lisiecki A (2018) Automated Laser Welding of AISI 304 Stainless Steel by Disk Laser. Arch Metall Mater 2018 Vol 63 No 4 1663-1672
19. Sisodia RPS, Gáspár M (2021) Investigation of Metallurgical and Mechanical Properties of Laser Beam Welded and Post-weld Heat Treated DP1400 Steel. J Mater Eng Perform 30:1703–1710. https://doi.org/10.1007/s11665-021-05469-x
20. Tuz L, Sokołowski Ł, Stano S, et al (2023) Effect of Post-Weld Heat Treatment on Microstructure and Hardness of Laser Beam Welded 17-4 PH Stainless Steel. Materials 16:. https://doi.org/10.3390/ma16041334
21. Liu Y, Wang J, Zhang W (2025) Effect of gap distance on forming and properties of laser welded joints of QP980/DP780 dissimilar steels. Weld World. https://doi.org/10.1007/s40194-025-02137-9
22. Vollertsen F, Grünenwald S (2008) Defects and process tolerances in welding of thick plates. In: ICALEO 2008: 27th International Congress on Laser Materials Processing, Laser Microprocessing and Nanomanufacturing. Laser Institute of AmericaLIA, Temecula, California, USA, p 1004
23. Volpp J, Frostevarg J (2021) Elongated cavities during keyhole laser welding. Mater Des 206:109835. https://doi.org/10.1016/j.matdes.2021.109835
24. Giudice F, Missori S, Sili A, et al (2024) Dissimilar Welding of Thick Ferritic/Austenitic Steels Plates Using Two Simultaneous Laser Beams in a Single Pass. J Manuf Mater Process 8:. https://doi.org/10.3390/jmmp8040134
25. Krishna Murthy KR, Sanei R, Sharma A, et al (2025) Impact of Beam Shape and Frequency on Weld Seam Geometry and Penetration Depth Using a Coherent Beam Combining Laser. Appl Sci 15:9432. https://doi.org/10.3390/app15179432
26. Horník P, Šebestová H, Novotný J, Mrňa L (2022) Laser beam oscillation strategy for weld geometry variation. J Manuf Process 84:216–222. https://doi.org/10.1016/j.jmapro.2022.10.016

27. Franco D, Oliveira JP, Santos TG, Miranda RM (2021) Analysis of copper sheets welded by fiber laser with beam oscillation. Opt Laser Technol 133:106563. https://doi.org/10.1016/j.optlastec.2020.106563

28. Grünenwald S, Unt A, Salminen A (2018) Investigation of the influence of welding parameters on the weld geometry when welding structural steel with oscillated high-power laser beam. Procedia CIRP 74:461–465. https://doi.org/10.1016/j.procir.2018.08.150

29. Kwieciński K, Lota K, Kiełbasiński M, et al (2022) Advanced Methods of Joining Battery Cells in the Automotive Industry. Bull Inst Weld 15–22. https://doi.org/10.17729/ebis.2022.5/2

30. Caprio L, Borzoni G, Previtali B, Demir AG (2022) Hand-Held Laser Welding of AISI301LN for components with aesthetic requirements: Toward the integration of machine and human intelligence. J Laser Appl 35:012008. https://doi.org/10.2351/7.0000746

31. Kumar A (2025) Exploring Manual Laser Oscillation Welding of Stainless Steel in Different Joint Configurations. Lasers Manuf Mater Process 12:1037–1060. https://doi.org/10.1007/s40516-025-00319-3

32. Wang Z, Oliveira JP, Zeng Z, et al (2019) Laser beam oscillating welding of 5A06 aluminum alloys: Microstructure, porosity and mechanical properties. Opt Laser Technol 111:58–65. https://doi.org/10.1016/j.optlastec.2018.09.036

33. Zhang C, Yu Y, Chen C, et al (2020) Suppressing porosity of a laser keyhole welded Al-6Mg alloy via beam oscillation. J Mater Process Technol 278:116382. https://doi.org/10.1016/j.jmatprotec.2019.116382

34. Fan Y, Cao J, Zhang J, et al (2024) Stable production of dissimilar steel joints in construction machinery by narrow gap oscillating laser welding. J Mater Res Technol 30:1403–1413. https://doi.org/10.1016/j.jmrt.2024.03.126

35. Zheng C, Yu W (2018) Effect of low-temperature on mechanical behavior for an AISI 304 austenitic stainless steel. Mater Sci Eng A 710:359–365. https://doi.org/10.1016/j.msea.2017.11.003

36. Landowski M, Łabanowski J, Jurkowski M (2025) Effect of solution heat treatment on mechanical properties of Manaurite XM reformer tubes after long term service at elevated temperatures. Adv Sci Technol Res J 19:220–228. https://doi.org/10.12913/22998624/200705

37. Monteiro SN, Nascimento LFC, Lima ÉP, et al (2017) Strengthening of stainless steel weldment by high temperature precipitation. J Mater Res Technol 6:385–389. https://doi.org/10.1016/j.jmrt.2017.09.001

38. Fan S, Jia L, Lyu X, et al (2017) Experimental investigation of austenitic stainless steel material at elevated temperatures. Constr Build Mater 155:267–285. https://doi.org/10.1016/j.conbuildmat.2017.08.047

39. Walczak M, Szala M, Okuniewski W, et al (2022) Assessment of Corrosion Resistance and Hardness of Shot Peened X5CrNi18-10 Steel. Materials 15:. https://doi.org/10.3390/ma15249000

40. Mao Z, Farkoosh AR, Seidman DN (2024) Effects of alloying elements on carbon diffusion in the austenite (f.c.c.) and ferrite (b.c.c.) phases

41. Zhao Y, Liu H-L, Wei L-L, Chen L-Q (2023) An overview on the novel heat-resistant ferritic stainless steels. Tungsten 5:467–480. https://doi.org/10.1007/s42864-022-00171-4

42. Szala M, Walczak M, Pałka T, et al (2025) Comparison of cavitation erosion and sliding wear resistance of welded CoCrWC and NiCrBSi hardfacings, AISI 316L stainless steel, and S235JR mild steel. Adv Sci Technol Res J 19:275–291. https://doi.org/10.12913/22998624/209577

43. Köse C, Topal C (2023) Dissimilar laser beam welding of AISI 2507 super duplex stainless to AISI 317L austenitic stainless steel. Mater Sci Eng A 862:144476. https://doi.org/10.1016/j.msea.2022.144476

44. Simon V, Varbai B, Abaffy K, Gyura L (2024) The Effects of Laser Power and Travel Speed on Weld Geometry in the case of Manual Laser Welding. Acta Mater Transylvanica 7:44–47. https://doi.org/10.33924/amt-2024-01-08

45. Pańcikiewicz K, Świerczyńska A, Hućko P, Tumidajewicz M (2020) Laser Dissimilar Welding of AISI 430F and AISI 304 Stainless Steels. Materials 13:4540. https://doi.org/10.3390/ma13204540

46. Danielewski H, Kurp P, Skrzypczyk A, et al (2025) Properties and Microstructure Evaluation of Laser-Welded TP347—TP904L High-Alloy, Stainless Steels Joints, Modified with 309L Filler. Materials 18:. https://doi.org/10.3390/ma18245633

47. Sathiya P, Abdul Jaleel MY (2011) Influence of shielding gas mixtures on bead profile and microstructural characteristics of super austenitic stainless steel weldments by laser welding. Int J Adv Manuf Technol 54:525–535. https://doi.org/10.1007/s00170-010-2967-x

48. Baghdadchi A, Hosseini VA, Hurtig K, Karlsson L (2021) Promoting austenite formation in laser welding of duplex stainless steel—impact of shielding gas and laser reheating. Weld World 65:499–511. https://doi.org/10.1007/s40194-020-01026-7

49. Farhadipour P, Dehghan S, Barka N, et al (2024) A study on effect of laser overlay welding parameters of stainless steel 301 LN: tensile test, microstructure analysis and microhardness evaluation. Weld Int 38:409–421. https://doi.org/10.1080/09507116.2024.2342342

50. Datta S, Raza MS, Muvvala G, et al (2023) The effect of different laser head angles and shielding gas supply systems to maximize the depth of penetration by minimizing the plasma shielding effect in fiber laser welding of 3-mm thick NiTinol sheet. Optik 283:170903. https://doi.org/10.1016/j.ijleo.2023.170903

51. Meng X, Putra SN, Bachmann M, et al (2024) A fundamental study of physical mechanisms of wineglass-shaped fusion zone profile in laser melting. J Mater Process Technol 324:118265. https://doi.org/10.1016/j.jmatprotec.2023.118265

52. Rogalski G, Świerczyńska A, Fydrych D (2023) Determination of t8/5 cooling times for underwater local dry welding of steel. Mar Struct 91:103477. https://doi.org/10.1016/j.marstruc.2023.103477

53. Giudice F, Sili A, Giudice F, Sili A (2021) Weld Metal Microstructure Prediction in Laser Beam Welding of Austenitic Stainless Steel. Appl Sci 11:. https://doi.org/10.3390/app11041463

54. Chamim M, Darmadi DB, Purnowidodo A, et al (2024) Influence of the welding thermal cycle on δ-ferrite evolution in the first layer of austenitic stainless steel (ASS) 308L produced by WAAM-GTAW. Case Stud Therm Eng 64:105489. https://doi.org/10.1016/j.csite.2024.105489

55. Gupta SK, Patil AP, Rathod RC, et al (2024) Cold Metal Transfer Welding of Ferritic and Austenitic Stainless Steel: Microstructural, Mechanical, and Electrochemical Studies. J Mater Eng Perform 33:10663–10679. https://doi.org/10.1007/s11665-024-09743-6

56. Teixeira RLP, Damasceno AIP, Nascimento R, et al (2026) Phase stability, microstructural evolution, and corrosion behavior of GTAW-welded AISI 316 L austenitic stainless steel. Mater Today Commun 50:114537. https://doi.org/10.1016/j.mtcomm.2025.114537

57. García-García V, Reyes-Calderón F, Frasco-García OD, Alcantar-Modragón N (2022) Mechanical behavior of austenitic stainless-steel welds with variable content of δ-ferrite in the heat-affected zone. Eng Fail Anal 140:106618. https://doi.org/10.1016/j.engfailanal.2022.106618

58. Muñoz JA, Dolgach E, Tartalini V, et al (2023) Microstructural Heterogeneity and Mechanical Properties of a Welded Joint of an Austenitic Stainless Steel. Metals 13:. https://doi.org/10.3390/met13020245

59. Pavan AR, Arivazhagan B, Vasudevan M, et al (2023) Study on the microstructure and mechanical properties of hybrid laser + MIG welded joints of 316LN stainless steel. Opt Laser Technol 163:109410. https://doi.org/10.1016/j.optlastec.2023.109410

60. Liu J, Nie Y, Feng Q, et al (2025) Influence of Welding Speed on the Microstructure and Mechanical Properties of Laser-Welded Joints in 316L Stainless Steel Sheets. Metals 15:. https://doi.org/10.3390/met15060624

61. Zhang C, Li X, Gao M (2020) Effects of circular oscillating beam on heat transfer and melt flow of laser melting pool. J Mater Res Technol 9:9271–9282. https://doi.org/10.1016/j.jmrt.2020.06.030